Unresolved Point Sources in the Galactic Center: An Unbinned Analysis using Wavelets with Injection Tests

Matthew R. Buckley,[1] Dan Hooper,[2] and Edward D. Ramirez[1]

[1]*Department of Physics and Astronomy, Rutgers University, Piscataway, NJ 08854, USA*
[2]*Fermi National Accelerator Laboratory*

We study the hypothesis that the excess of γ-rays in the Galactic Center is produced by a population of unresolved point sources. We do this by applying a wavelet-based algorithm that locates and infers the properties of the point sources, without requiring a background model. To study the performance of the algorithm, we first consider how well it identifies point sources injected into a simulated background representative of the diffuse emissions detected by Fermi-LAT. Then, we apply the algorithm to real data to construct a catalog of point sources and set new limits on the luminosity of an unresolved population of point sources. Unlike previous wavelet-based studies, this analysis is unbinned in space and test the algorithm with injection tests on the real data.

I. INTRODUCTION

- The Galactic Center Excess
- Unresolved Point Source Hypothesis of Excess
- Detected point sources
- Nonpoissonian Stats
- Wavelet Analysis
- Motivation for wavelet injection tests given its importance in the interpretation of Nonpoissonian stats
- Brief outline of paper

II. FERMI-LAT DATA

- Data description
- Point source population
- Diffuse emission models
- Data selection (commented, merged with data description)
- PSF

Description of the Data. We use Pass 8 data from Fermi-LAT, version P8R3**(_V2?)** recorded from 4 Aug 2008 to 20 Feb 2019 (weeks 9-559 of Fermi-LAT observations). From the dataset, we select CLEAN-FRONT (or ULTRACLEAN-FRONT) converted data with the filters ___. Our photons span the energy range of ___ to ___. The maps are binned in energy from 100MeV to 10^9MeV The data is expected to be sourced by several diffuse emission components and point sources—sources of photons that are localized at scales smaller than the standard deviation of the Fermi-LAT PSF.

Diffuse emission models. Much of the observed photons are expected to form via processes spread diffusely across the sky. Several diffuse emission template models are used to explain this: (i) neutral pion decay, (ii) inverse-Compton scattering of leptons (isotropic and anisotropic), (iii), bremsstrahlung emission from leptons, (iv) synchrotron emission, and (v) emission from the Fermi Bubbles. [2.2: 1704.03910].

More detailed description if necessary.

Point source population. The most recent population of point sources identified is given by the Fermi-4FGL catalog.

More detailed description.

Presence of GCE after Fit (See Fig. 1 from Zhong et al.)

Fermi PSF. The Fermi-LAT cannot perfectly determine the direction $\hat{v}$ at which an incoming photon emanated from. Instead, it will determine a reconstructed direction $\hat{v}' = \hat{v} + \delta v$, whose probability distribution is governed by the point-spread function (PSF), $P(\delta v|E, \hat{v})$. To scale out the energy-dependence from the PSF, one defines the *scaled angular deviation* x, given by

$$x = \frac{\delta v}{S_P(E)}, \tag{1}$$

where the *scaling function* $S_P(E)$ is given by

$$S_P(E) = \sqrt{\left(c_0 \left(\frac{E}{100 \text{ MeV}}\right)^{-\beta}\right)^2 + c_1^2}. \tag{2}$$

For FRONT events, the parameters $c_0 = 6.38 \times 10^{-2}$, $c_1 = 1.26 \times 10^{-3}$, and $\beta = 0.8$[1]. The PSF can then be written as $P(x|\hat{v})$.

For the **P8R3_V2** dataset, the PSF is fit to the following function:

$$P(x|E) = f_{\text{core}} K(x, \sigma_{\text{core}}, \gamma_{\text{core}}) + (1 - f_{\text{core}}) K(x, \sigma_{\text{tail}}, \gamma_{\text{tail}}), \tag{3}$$

where the parameters $\{f_{\text{core}}, \sigma_{\text{core}}, \ldots\}$ are each functions of energy and K is the King function, given by

$$K(x, \sigma, \gamma) = \frac{1}{2\pi\sigma^2} \left(1 - \frac{1}{\gamma}\right) \left(1 + \frac{x^2}{2\gamma\sigma^2}\right)^{-\gamma}. \tag{4}$$

Questions:

1. Where did the dependence on $\hat{v}$ go? Authors note that dependence is on the LAT-boresight angle

III. DETECTION STRATEGY

A. Wavelets

- General discussion on wavelets
- Unresolved Point Source Hypothesis of Excess
- Detected point sources
- Nonpoissonian Stats
- Wavelet Analysis
- Motivation for wavelet injection tests given its importance in the interpretation of Nonpoissonian stats
- Brief outline of paper

General Discussion. Wavelets are a class of functions that can be used to study features of functions or images at multiple scales. Similar to the way the Fourier transform is used to study features in frequency space, the continuous wavelet transform can be used to study features in both frequency and position space. This is particularly useful for point source detection, as they are both small-scale fluctuations located within a small region of space.

As we are studying γ-rays, the data exists on the 2D sphere and hence has a PDF $f(\vec{x})$ associated with it. In principle, this PDF would contain contributions from unresolved point sources if they exist. Therefore, the PDF is our object of study. Given a real-valued wavelet $\psi(\vec{x})$, the *continuous wavelet transform* w is a convolution of the function f with the wavelet ψ:

$$w(\vec{x}, a) = \frac{1}{a} \int d^2x' f(\vec{x}') \; \psi\left(\frac{\vec{x} - \vec{x}'}{a}\right), \tag{5}$$

---

[1] https://fermi.gsfc.nasa.gov/ssc/data/analysis/documentation/Cicerone/Cicerone_LAT_IRFs/IRF_PSF.html

where the integral is taken over the entire space such as $\mathbb{R}^2$ or the sphere and the non-negative parameter a specifies the scale of the features that are picked out by the wavelet.

The choice of wavelet for analysis depends on which features one is studying. Previous works have employed the Mexican Hat wavelet family for point source detection. For our work, we use the Mexican hat wavelet of the first kind:

$$\psi(\vec{x}) = (2 - x^2)\ e^{-x^2/2} \tag{6}$$

The advantage of this wavelet is seen from its shape. Its central peak makes it suitable for detecting Gaussian-like functions and its negative tails perform a kind of background subtraction when computing the CWT. At a deeper level, it is sensitive to the max/min of the function that it transforms and filters out constant/linear functions. This follows from this wavelet being the Laplacian of a Gaussian since, through integration by parts, the CWT of a function can be written as the second derivative of the function convolved with a Gaussian filter, due to the wavelet's expression as a Laplacian of a Gaussian.

Wavelet Analysis. We search for point sources across the entire sky. First, we partition the sky into 192 equal-area ($\sim 10^\circ$) regions using the HEALPix pixelization scheme. We do this by setting NSIDE = 4. We refer to these regions as *father pixels*. Since these father pixels have small angular extent, projecting their datapoints into the tangent plane of the father will not significantly affect the distances between datapoints. Therefore, we can employ flat 2D wavelets in these projected father pixels to perform our wavelet analysis, as opposed to employing generalizations of wavelets to the sphere.

Within a projected father pixel we will have N samples $\{\vec{x_k}\}_{k=1}^N$ of reconstructed photon positions with an underlying theoretical distribution $f(\vec{x})$. The CWT can be estimated with a sample mean

$$w(\vec{x}, a) \sim \frac{1}{a} \sum_{k=1}^{N} \psi\left(\frac{\vec{x} - \vec{x}_k}{a}\right). \tag{7}$$

Unlike previous approaches, this estimation of the wavelet coefficients does not require binning the data.

A direct implementation of the wavelet transformation at this point would lead to issues at the edges, since the transformation would determine the sharp drop in photons at the edges as intense small-scale fluctuations. Therefore, we extend our integration domain by integrating over points $\sim 4^\circ$ away from the edges (projected into the same tangent plane). This extension is much longer than the effective support **(define in General Discussion once you calculate the WT of the PSF)** of the wavelet at the scales of interest, so this gives a good estimate of the true CWT.

Point Sources as Peaks in the Wavelet Map.

Post-Processing.

Source Properties.

IV. MONOCHROMATIC WAVELET ANALYSIS ON SIMULATED DATA

V. BINNED ENERGY WAVELET ANALYSIS ON SIMULATED DATA

VI. WAVELET ANALYSIS ON REAL DATA.

VII. DISCUSSION.

VIII. CONCLUSIONS.

IX. BACKGROUND

Wavelet analyses of the Galactic center excess have been attempted before.

Zhong et al 1911.12369 performs a template fit to the GCE, and then uses a masked filter algorithm based on a Mexican hat function

$$M_2(\vec{x}, \sigma) = \frac{e^{-|\vec{x}|^2/2\sigma^2}}{16\pi\sigma^4} \left[\left(\frac{|\vec{x}|^2}{\sigma^2} - 4\right)^2 - 8\right] \tag{8}$$

with a figure of merit defined at a location through the convolution $\mathcal{F}$ of M_2 with the pixelized photon count map

$$S[\mathcal{C}] = \frac{\mathcal{F}[M_2]}{\sqrt{\mathcal{F}[(M_2)^2]}}. \tag{9}$$

Here, σ is Galactic latitude dependent:

$$\sigma = (0.4^\circ) \times (0.53 + 0.3|b|/12^\circ). \tag{10}$$

This matched filter is applied to the region $2^\circ \leq |b| \leq 12^\circ$, $|\ell| \leq 12^\circ$, in the energy range $1 < E_\gamma < 4$ GeV, in annuli of width 3°, with GALPROP background maps binned in $0.1^\circ \times 0.1^\circ$ bins. The GALPROP model is varied over 60 parameters, and 100 iterations are used to generate the non-point source distribution of the $S[\mathcal{C}]$ statistic. I do not see that they performed injection tests of point sources. They find a distribution of test statistic in the data compatible with a smooth background once the 4FGL point source mask was applied. A study of the luminosity function is done, but I don't see a clear plot connecting luminosity with expected $S[\mathcal{C}]$.

Bartels et al 1506.05104 previously used the $S[\mathcal{C}]$ figure of merit later adopted by Zhong et al. They simulated point sources with spherically symmetric distribution around the Galactic Center, and a photon distribution of

$$\frac{dN}{dE} \propto e^{-E/3.78\ \mathrm{GeV}} E^{-1.57} \tag{11}$$

and a luminosity function

$$\frac{dN}{dL} \propto L^{-1.5}. \tag{12}$$

They use the same region of interest and energy range as Zhong et al later reanalyze. These point sources are injected into simulated background to determine an expected distribution of $S[\mathcal{C}]$ (see Figure 2).

X. SIMULATED DATA

A. Point Spread Function

FIG. 1: Gaussian σ fit to PSF from FermiPy (blue) and the best-fit function Eq. (**??**) (red).

B. GALPROP Background

I use Anastasia's GALPROP backgrounds **Need details on the GALPROP model and choices going in to this**. Our model does not yet contain the Fermi Bubbles **need to add this**. Maps are binned in energy, from 100 MeV to 10^9 MeV, with a logarithmic binning (each bin scaled by $\log_{10} 60$). The GALPROP maps are binning using HealPy with `nsides=256`. Each pixel therefore corresponds to approximately 1.6×10^{-5} sr, or an angular size of 0.04 radians in extent.

There appears to be a normalization issue in the GALPROP maps across energy

In Figure 2 I show 6 of the 29 background maps. Note these maps do not

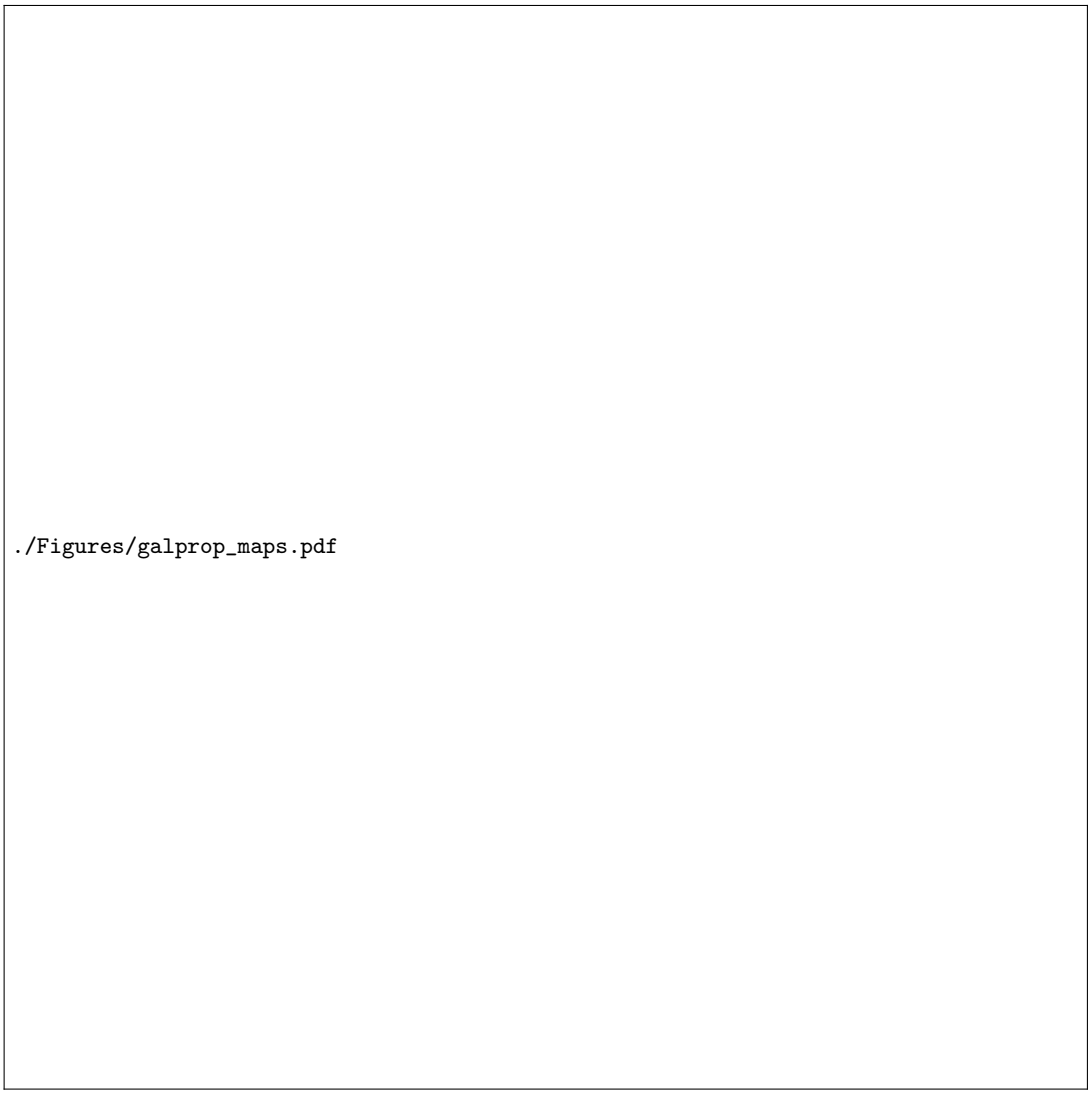

FIG. 2: Selected GALPROP background flux maps $E^2\Phi$, in units of $\mathrm{MeV}^2/\mathrm{cm}^2/\mathrm{sr/s/MeV}$.

C. Point Source Identification with Wavelets

D. Correlating Energy Bins

Appendix A: The Continuous Wavelet Transform of a Gaussian

Appendix B: The Continuous Wavelet Transformation of the King Profile

For the King Profile given by Eq. (4) and the Mexican Hat wavelet of the first kind given by Eq. (6), its continuous wavelet transform can be given by the following integral expression over the radius b:

$$w(\vec{b},a) = \frac{(1-\gamma^{-1})}{\sigma^2 a} e^{-b^2/2a^2} \int_0^\infty dx\; x \left(1+\frac{x^2}{2\sigma^2\gamma}\right)^{-\gamma} e^{-x^2/2a^2} \left[\left(2-\frac{b^2}{a^2}-\frac{x^2}{a^2}\right) I_0\left(\frac{bx}{a^2}\right) + \frac{2bx}{a^2} I_1\left(\frac{bx}{a^2}\right)\right], \quad \text{(B1)}$$

where I_0 and I_1 are the modified Bessel functions of the zeroth and first kinds, respectively. We evaluate the function by performing a numerical integral via Gaussian quadrature[2]. Requiring a computer to solve this integral directly through Gaussian quadrature fails due to the exponentially increasing values of the modified Bessel functions. Therefore, when bx/a^2 exceeds some high enough value before the algorithm fails, we replace the modified Bessel functions with their asymptotic expansions[3]:

$$I_0(x) \sim \frac{e^x}{\sqrt{2\pi x}}\left(1+\frac{1}{8x}\right) \;;\; I_1(x) \sim \frac{e^x}{\sqrt{2\pi x}}\left(1-\frac{3}{8x}\right) \tag{B2}$$

Therefore, we can rewrite the integral as

$$w(\vec{b},a) \sim \frac{(1-\gamma^{-1})}{\sigma^2 a}\Bigg\{e^{-b^2/2a^2}\int_0^R dx\; x\left(1+\frac{x^2}{2\sigma^2\gamma}\right)^{-\gamma} e^{-x^2/2a^2}\left[\left(2-\frac{b^2}{a^2}-\frac{x^2}{a^2}\right)I_0\left(\frac{bx}{a^2}\right)+\frac{2bx}{a^2}I_1\left(\frac{bx}{a^2}\right)\right]+ \tag{B3}$$

$$+\int_R^\infty dx\; x\left(\frac{a}{\sqrt{2\pi bx}}\right)\left(1+\frac{x^2}{2\sigma^2\gamma}\right)^{-\gamma} e^{-(x-b)^2/2a^2}\left[\left(2-\frac{b^2}{a^2}-\frac{x^2}{a^2}\right)\left(1+\frac{1}{8}\frac{a^2}{bx}\right)+\frac{2bx}{a^2}\left(1-\frac{3}{8}\frac{a^2}{bx}\right)\right]\Bigg\}, \tag{B4}$$

where R represents the value at which we begin replacing the true integrand with its asymptotic approximation.

This would be enough if $\vec{x}$ denotes the raw angular deviation. However, the PSF is in terms of the scaled angular deviation in Eq. (1). Therefore, the King distribution in terms of the raw angular deviation is given by

$$P_r(r) = P_x(x(r))\frac{dx}{dr} = \frac{1}{S_P(E)}\; P_x(r/S_P(E)) \tag{B5}$$

Therefore, the only modification to the wavelet expression above is to make is in the King Profile term by replacing $x \to x/S_P(E)$ and divide the entire expression by $S_P(E)$. Thus,

$$w(\vec{b},a) = \frac{1}{S_P(E)}\frac{(1-\gamma^{-1})}{\sigma^2 a}e^{-b^2/2a^2}\times \tag{B6}$$

$$\times\int_0^\infty dx\; x\left(1+\frac{x^2/S_P^2(E)}{2\sigma^2\gamma}\right)^{-\gamma} e^{-x^2/2a^2}\left[\left(2-\frac{b^2}{a^2}-\frac{x^2}{a^2}\right)I_0\left(\frac{bx}{a^2}\right)+\frac{2bx}{a^2}I_1\left(\frac{bx}{a^2}\right)\right], \tag{B7}$$

Since the major issues with the Gaussian quadrature were related to the modified Bessel functions, the algorithm should have no problem computing this modified integral.

For the full PSF, we simply use the linearity of the CWT applied to a sum of two King profiles.

As a test of accuracy, we verify the fact that the CWT of the King profile should approach that of a Gaussian with the same σ-parameter as $\gamma \to \infty$, as the King profile converges to the Gaussian in this limit. In Fig. **??** plot the CWT of the King profile with $\sigma = 0.1$ and varying γ-values and the Gaussian with $\sigma = 0.1$ at the scale $a = 0.1$. As expected, the CWTs agree. Moreover, the CWT behaves as expected. Since the King's tail survives longer than that of the Gaussian at the expense of its peak, the CWT should be less pronounced at the peak and be more spread out.

As in the Gaussian case, the intensity and size of a King source can be inferred from the maximum CWT value of the source. In that case, the scale giving the maximum CWT is $a_{max} = \sqrt{3}\sigma$ and the maximum (rescaled) CWT obeys $a \times w_0(a_{max}) = 9/8$. However, with extra parameters, we expect the relationship between source properties and the CWT to be dependent on these parameters. Empirically, we see that the CWT is maximum at $\vec{b} = \vec{0}$ for all a (it is also easily shown to be a critical point of the CWT). In that case, the CWT can be written as

$$w_0(a) = \frac{2(\gamma-1)}{a}\left[-1+\gamma\; e^{\gamma q}\;(1+q)\;E_\gamma(\gamma q)\right], \tag{B8}$$

where $q = \sigma^2/a^2$ and $E_\nu(z)$ denotes the generalized exponential integral function given by

$$E_\nu(z) = \int_1^\infty dt \frac{e^{-zt}}{t^\nu}. \tag{B9}$$

---

[2] Mathematica's NIntegrate function seems to perform this integral quite easily

[3] https://math.stackexchange.com/questions/2791588/leading-terms-in-asymptotic-expansion-of-modified-bessel-function-of-the-fir ; https://functions.wolfram.com/Bessel-TypeFunctions/BesselI/06/02/01/01/01/0001/ ; Gradsteyn 8.451.5

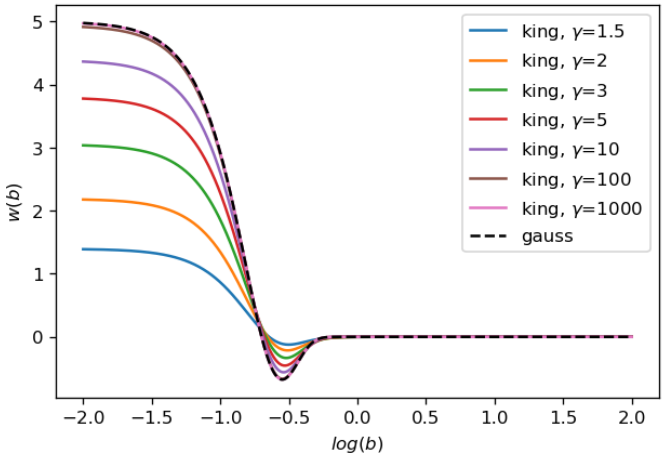

FIG. 3: Comparison between the CWT of the King profile with $\sigma = 0.1$ and varying γ-values and the Gaussian with $\sigma = 0.1$ at the scale $a = 0.1$. (source: od/pswavelets/gce/matt_post_energy/wavelet_transform_king.ipynb)

Note, since the CWT depends on σ only through the ratio $q = \sigma^2/a^2$, then we expect the King profile's maximum CWT to occur at $a_{max} \propto \sigma$, as in the Gaussian case, except with a possibly different normalization. This is not sufficient as a proof, though we have verified our claim numerically (see Fig. 4). A proof follows from observing the behavior of the critical points:

$$0 = \partial_a \frac{f(\sigma/a)}{a} = \frac{-f'(\sigma/a) \times (\sigma/a) - f(\sigma/a)}{a^2}, \tag{B10}$$

where f here would represent our rescaled CWT and f/a represents the original CWT. Therefore, the location of the critical point is entirely determined by σ/a, so all critical points take the form $a_c \propto \sigma$. This results means that the $a_{\max}$ is entirely determined by the term in the square brackets Eq. (B8) and so the rescaled CWT $a \times w_0(a)$ depends only on a through the parameter σ/a. For the following tests, it is then sufficient to take $\sigma = 1$, which only affects the value of $a_{max} \propto \sigma$.

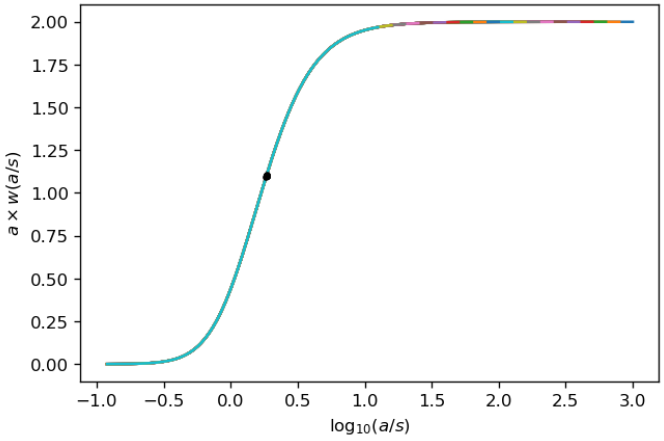

FIG. 4: Rescaled CWT versus the ratio a/σ for a range of σ-values and $\gamma = 1.5$ (non-trivial case). What we find is what we proved: the maxima corresponding to all σ-parameters collapse to a single point in the graph. (source: od/pswavelets/gce/matt_post_energy/max_cwt_king.ipynb)

The parameter we have neglected so far is γ. As may be guessed from Eq. (B8), it will affect both the maximum CWT value and the maximum scale parameter, affecting how we determine the source size and counts. To test this, we estimate $a_{\max}$ and $w_0(a_{\max})$ by calculating in a grid of a- and γ-values. The results are shown in Fig. 5. Notice that the results approach the Gaussian results smoothly as $\gamma \to \infty$.

It is difficult to fit these relations analytically, so we will simply interpolate in the future. In practice, we do not need to consider values of γ in the extreme cases $\gamma \sim 1$ and $\gamma \sim \infty$, where we begin to encounter numerical instabilities.

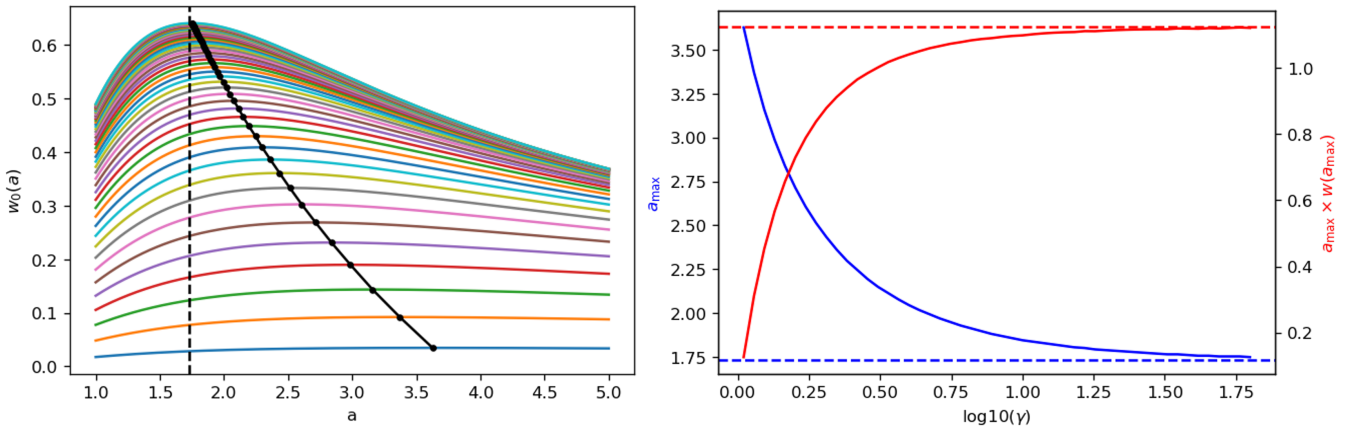

FIG. 5: *(Left)* Peak CWT versus scale parameter for a range of γ and $\sigma = 1$. The Gaussian limit for a_{max}, $\sqrt{3}\sigma$, is denoted by the dashed line. *(Right)* The blue curve shows how a_{max} depends on γ for the range considered. The horizontal blue-dashed line denotes the Gaussian limit $\sqrt{3}\sigma$. The red curve shows how the rescaled peak CWT depends on γ, where the Gaussian limit (9/8) is denoted by the red-dashed horizontal line. (source: od/pswavelets/gce/matt_post_energy/max_cwt_king.ipynb)

For the fit that Zhong gave us for the CLEAN data, we need only take $\gamma_{min} \sim 1.5$ and $\gamma_{max} \sim 12$, where the results are stable enough.

There are two issues left: (1) photons will have different energies, (2) the PSF is a sum of two King profiles, requiring more parameters that would affect the value of a_{max} and $w_0(a_{max})$. For the first problem, the best thing to do would be to restrict ourselves to a bin of energy and average in energy. Or, use $a_{\rm max}$ optimized for point source detection, then find relation between wavelet coefficient and number of counts analytically or using MC simulations. For the second problem, the issue may require us to take a weighted average of both a_{max}, weighted by the fraction in either distribution or more complicated fitting. However, in the GeV range, the core distribution dominates, so we may be fine just taking the a_{max} corresponding to the core.

Appendix C: Background Probabilities

Uniform (+ linear) background [1, 2] Look-up table for low counts GAussian fit for high counts (fit formulas in both references)

Appendix D: Efficiently Generating Samples of the PSF

To sample angular deviations from the PSF, we first sample the scaled angular deviation x given by Eq. (1). To do this, we first note that, though the PSF Eq. (3) is difficult to efficiently sample from, we can perform inverse transform sampling to sample from a single King profile.

We perform the inverse transform sampling by first writing the King profile as a PDF in x only (not x and ϕ. This simply removed a factor of 2π from the profile.

$$K_x(x, \sigma, \gamma) = 2\pi x \times K(x, \sigma, \gamma) \tag{D1}$$

In this way, it is unambiguous to define the CDF of the 1D King profile:

$$F(x) = 2\pi \int_0^x dx' \; x' \; K(x', \sigma, \gamma) \tag{D2}$$

$$= 1 - \frac{1}{(1 + \frac{x^2}{2\gamma\sigma^2})^{\gamma - 1}} \tag{D3}$$

Inverting this function for $x(F)$, we have

$$x(F) = \left\{ 2\gamma\sigma^2 \left[(1 - F)^{-1/(\gamma - 1)} - 1 \right] \right\}^{1/2}, \tag{D4}$$

which implies that we can generate random samples of the King distribution using

$$x \sim \left\{ 2\gamma\sigma^2 \left[(1 - U[0,1)])^{-1/(\gamma-1)} - 1 \right] \right\}^{1/2}. \tag{D5}$$

To sample from the PSF Eq. (3), the sampling algorithm is straightforward.

1. Generate empty sample array of length N
2. Generate N samples from the "core" King distribution
3. Generate N samples from the "tail" King distribution
4. Taking the fraction $f_{\rm core}$ to be the discrete probability that a sample lies in the "core" distribution as opposed to the "tail" distribution, generate N outcomes corresponding to Bernoulli trials with success probability $f_{\rm core}$. In practice, this is done by generating the following Boolean quantity:

$$U[0, 1, \text{size} = \text{N}) \leq f_{\rm core}$$

5. The nth-entry of sample array is given by the nth-entry of the "core" array if the nth-entry of the Boolean quantity is True. Otherwise, it is taken from the "tail" array.

This is algorithm is efficient as it depends almost entirely on analytic operations and may be vectorized. As a check that this produces a correct set of samples, we consider a realization of the distribution for some set of parameters and compare the output of the algorithm to the output of a simple (and inefficient) rejection sampling algorithm (Ziggurat). The rejection sampling algorithm is very simple: generate a point uniformly on a square enclosing the graph of the PDF, check that each point is above or below the PDF, if below then it is taken as a sample, if below, then it is note. We iterate the process until we get the desired amount of samples. The result of this test is given in Fig. 6.

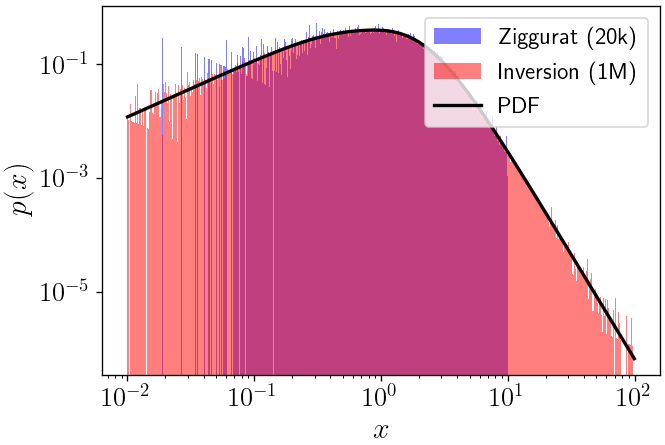

FIG. 6: Comparison between random samples produced using rejection sampling (Ziggurat) and inverse transform sampling with the true PSF for a set of parameters: $(\sigma_{\rm core}, \gamma_{\rm core}, \sigma_{\rm tail}, \gamma_{\rm tail}, f_{\rm core}) = (0.29874637,\ 3.07534477,\ 0.90834872,\ 2.34244808,\ 0.928262737)$. These parameters correspond to $E = 1\ GeV$ and a cubic fit (with respect to energy) of the fit parameters that Zhong provided us. Number of samples generated are indicated. Ziggurat method generated samples from 0 to 10, and so it appears truncated. (source: od/pswavelets/gce/matt_post_energy/psf_fitting_king_zhong.ipynb)

It should be possible for this code to remain efficient and vectorized even when we account for the non-trivial energy-dependence of the fit parameters. After generating samples of x, the next step is to multiply all samples by their associated scaling factor $S_P(E)$ to produce a sample of angular deviations $\delta\hat{v}$, again something that may easily be vectorized.

Appendix E: Wavelet Comparisons

Compare performance of Mexh 1 to Mexh 2 [3] and Bartels S-function [4]. First using single injection into background then multisource.

---

[1] F. Damiani, A. Maggio, G. Micela, and S. Sciortino, The Astrophysical Journal **483**, 350 (1997), ISSN 0004-637X.

[2] P. E. Freeman, V. Kashyap, R. Rosner, and D. Q. Lamb, The Astrophysical Journal Supplement Series **138**, 185 (2002), ISSN 0067-0049.

[3] F. Argüeso, J. González-Nuevo, J. L. Sanz, L. Toffolatti, P. Vielva, D. Herranz, and M. López-Caniego, 13th European Signal Processing Conference, EUSIPCO 2005 **000**, 325 (2005), 0604376.

[4] R. Bartels, S. Krishnamurthy, and C. Weniger, Physical Review Letters **116**, 1 (2016), ISSN 10797114, 1506.05104.